

Physical Biology



PAPER

Model reduction for stochastic CaMKII reaction kinetics in synapses by graph-constrained correlation dynamics

OPEN ACCESS

RECEIVED

31 October 2014

REVISED

3 April 2015

ACCEPTED FOR PUBLICATION

7 April 2015

PUBLISHED

18 June 2015

Content from this work may be used under the terms of the [Creative Commons Attribution 3.0 licence](#).

Any further distribution of this work must maintain attribution to the author(s) and the title of the work, journal citation and DOI.

Todd Johnson¹, Tom Bartol², Terrence Sejnowski² and Eric Mjolsness¹¹ Department of Computer Science, University of California Irvine CA 92697, USA² Salk Institute, La Jolla CA, USAE-mail: johnson.todd@gmail.com, bartol@salk.edu, sejnowski@salk.edu and emj@uci.edu**Keywords:** model reduction, stochastic reaction networks, rule-based modeling, graph-constrained correlation dynamics, Boltzmann learning, CaMKII, spike timing dependent plasticitySupplementary material for this article is available [online](#)**Abstract**

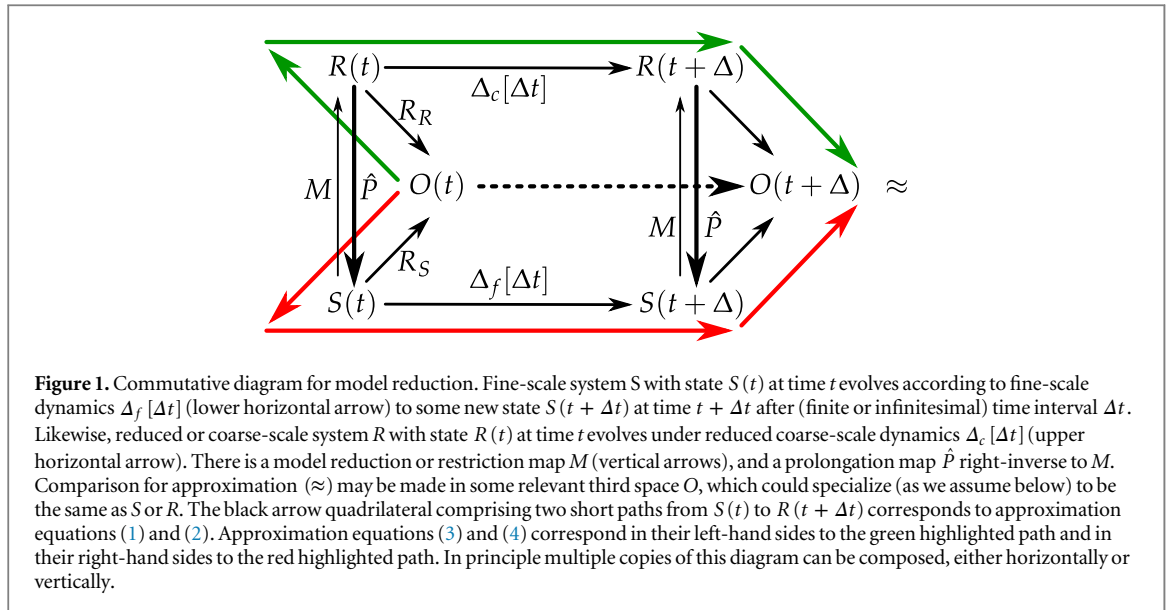
A stochastic reaction network model of Ca^{2+} dynamics in synapses (Pepke *et al* *PLoS Comput. Biol.* **6** e1000675) is expressed and simulated using rule-based reaction modeling notation in dynamical grammars and in MCell. The model tracks the response of calmodulin and CaMKII to calcium influx in synapses. Data from numerically intensive simulations is used to train a reduced model that, out of sample, correctly predicts the evolution of interaction parameters characterizing the instantaneous probability distribution over molecular states in the much larger fine-scale models. The novel model reduction method, ‘graph-constrained correlation dynamics’, requires a graph of plausible state variables and interactions as input. It parametrically optimizes a set of constant coefficients appearing in differential equations governing the time-varying interaction parameters that determine all correlations between variables in the reduced model at any time slice.

1. Introduction

Given a stochastic reaction network, even one specified by high-level ‘parameterized reactions’ or ‘rule-based’ notation [2–6], there is a corresponding chemical master equation (CME) for the evolution of probability distributions over all possible molecular states of the system. These states are ultimately described in terms of discrete-valued random variables. Unfortunately as the number of such random variables grows, the number of molecular states appearing directly in the CME grows exponentially. On the other hand even for a dynamical system that is nonlinear in its observable variables, the CME is a (very large) system of linear differential equations for time-evolving probabilities. The exponential explosion of state space size with number of random variables can often be bypassed in sampling-style simulation (such as the Gillespie stochastic simulation algorithm (SSA) [7] and its many variants), and also to a lesser extent for reaction rate inference, provided that enough trajectories are sampled to evaluate a required expected value. But the sampling approach

requires a lot of computing power to sample enough trajectories, and also poses substantial obstacles for analysis.

The problem of state space growth is compounded in the case of rule-based stochastic models [2, 4–6] since in that case even the number of molecular species suffers an exponential growth in terms of natural problem size parameters such as the number of binding sites in a molecular complex. Then the state space described in the master equation grows doubly exponentially in such problem size parameters, and it can be hard to really understand the resulting stochastic dynamical system. And yet, molecular complexes with combinatorially many states (such as transcription complexes, signal transduction complexes, and allosteric enzyme complexes) are ubiquitous in biology, so the problem cannot simply be avoided. For example, the signal transduction cascade in response to calcium influx through n-methyl D-aspartate receptors (NMDARs) in synapses, which plays a key role in synaptic plasticity in spatial learning and memory in mice, has such combinatorially generated number of local states of molecular complexes involving calcium,



calmodulin, CaMKII and phosphorylation sites, as will be described in section 3.1 below ([1, 8], and references therein). Each of the many possible states of each complex is itself a ‘molecular species’ with associated reaction channels.

To address these problems of model size and state space size, *reduced models* may have substantial advantages. In general, model reduction replaces a large model with a smaller and more tractable model that approximates the large model in some relevant aspect. The ideas of model ‘size’, ‘tractability’, ‘approximation’, and ‘relevant aspect’ can be defined in various ways. We will suggest one framework for these definitions in section 2.1 below. In sections 2.2 and 2.3 below we use this framework to introduce a new model reduction method for stochastic biochemical networks which in our target application are also rule-based, though they need not be.

Our method can be viewed as a form of ‘moment closure’ method as will be explained in section 2.4, which also contains further comparisons to related work. Compared to other methods of moment closure we seek a much more aggressive reduction in the model size, as counted by the number of degrees of freedom (chemical or biological variables with dynamically changing values) required *even in a sampling approach*, such as SSA, to the original unreduced biochemical model. This claim is substantiated in sections 2.4 and 3.4 below. Such a strategy may be appropriate to the eventual goal of finding usable ‘phenomenological’ but mechanistically well-founded approximate models of fine-scale subsystems to place within yet larger super-system models, for example placing calcium signal pathway reduced models within neuronal-level synaptic plasticity simulations, although we have not yet attempted such an application of this method. Unlike most but not all other

moment closure approaches, we retain (approximations to) correlations of arbitrarily high order rather than truncating them to zero. Our approach applies naturally to the case of rule-based models. And perhaps most importantly from the biological point of view, it is based on a problem-specific graph of possible interactions between key system variables. Such a graph is a natural place to impose human biological expertise on the approximate model reduction method.

2. Theory

2.1. Model reduction criteria

Figure 1 illustrates our general setting. The basic idea is that the results of following the red arrows around from earlier to later observations, by way of a fine-scale predictive dynamical model as one would do in an ordinary simulation, should approximately agree with the results of following the green arrows around through a coarse-scale model instead. Since the coarse-scale model is smaller, following the green arrows could be cheaper computationally and also more amenable to human understanding of the dynamics. To define this possibility technically, figure 1 also includes mappings M and \hat{P} directly between the fine-scale and coarse-scale model state spaces.

All vectors and maps defined below are assumed to be defined in the sense of probability distributions, so that for example the fine-scale system state vector $S(t)$ is a distribution over all possible individual microscopic states s . In the deterministic limit that distribution could be a delta function that picks out one winning microstate. Likewise maps M , $\Delta_f[\Delta t]$ etc take distribution vectors to distribution vectors. The forward time-evolution maps $\Delta_f[\Delta t]$ and $\Delta_c[\Delta t]$ are

linear on probability distributions, and thus preserve mixtures, but in this paper we do not assume linearity of M or the other maps introduced below.

Fine-scale and (reduced) course-scale dynamics are illustrated in figure 1. A model-reduction or ‘restriction’ map M should ideally *commute*, at least approximately, with time-evolution maps $\Delta_f [\Delta t]$ and $\Delta_c [\Delta t]$; thus for example

$$\Delta_c [\Delta t] \circ M \cdot S(t) \approx M \circ \Delta_f [\Delta t] \cdot S(t), \quad (1)$$

for all $S(t)$ or more strongly for almost all possible S , which in operator space could be stated as

$$\Delta_c [\Delta t] \circ M \approx M \circ \Delta_f [\Delta t]. \quad (2)$$

We will omit operator-space variants of the approximation statements below but they should be clear if the same vector appears at the rightmost end of each side of the approximation. Here and in this section the sense of approximation \approx has yet to be defined but it requires aggregating some measure of error over microstates s , r , or o . For deterministic systems, sum-of-squares error over dynamical variables is plausible; for stochastic systems, an asymmetric Kullback–Leibler (K–L) divergence or relative entropy between two distributions over system states is plausible. The K–L divergence is useful when approximating probability distributions because (a) it measures the extra information contained in one distribution beyond what is in a second distribution, and (b) it takes its minimal value, zero, when the two distributions are equal almost everywhere.

Equations (1) and (2) are not entirely satisfactory since they provide no control over the space in which approximation comparisons are to be made. Alternatively to equation (1), and adopting terminology used in multigrid/multiscale algorithms [9, 10], one could introduce a ‘prolongation’ map \hat{P} that is exactly or approximately right-inverse to M (so that $M \circ \hat{P} = I$ or $M \circ \hat{P} \approx I$), and make the commutativity comparison in the fine-scale system space, S , rather than course-scale, R . But a more general scheme that encompasses both alternatives is to compare time-evolved states or probability distributions on states in a third space of significant ‘observables’, $O(t)$, as shown, using restriction maps $R_S : S \rightarrow O$ (and its right powerset inverse or prolongation map P_S for which $R_S \circ P_S = I$) and $R_R : R \rightarrow O$ (and its right powerset inverse or prolongation map P_R for which $R_R \circ P_R = I$ if space R is not smaller than O so that R_R can be surjective) that predict the targeted observables based on the current state of each system. Then we seek

$$\begin{aligned} R_R \circ \Delta_c [\Delta t] \circ P_R \cdot O(t) \\ \approx R_S \circ \Delta_f [\Delta t] \circ P_S \cdot O(t), \end{aligned} \quad (3)$$

as illustrated by the red and green three-arrow paths in figure 1. This, or the corresponding operator statement in the O space:

$$R_R \circ \Delta_c [\Delta t] \circ P_R \approx R_S \circ \Delta_f [\Delta t] \circ P_S \quad (4)$$

is our most general statement of the commutation condition.

If we initialize $O(t) = R_S \cdot S(t)$, and assume for consistency the triangular commutation relation $P_R \circ R_S = M$, and define the projection operator $\Pi_S = P_S \circ R_S$, then equation (3) becomes

$$\begin{aligned} R_R \circ \Delta_c [\Delta t] \circ M \cdot S(t) \\ \approx R_S \circ \Delta_f [\Delta t] \circ \Pi_S \cdot S(t). \end{aligned} \quad (5)$$

Two special cases are salient for our computational experiments. In the special case $O = S$, which we will use, then $R_S = I$, $R_R = \hat{P}$, $P_S = I$ and $P_R = M$, (note R_R and P_R exchange roles so that $R_R \circ P_R \neq I$ but instead $P_R \circ R_R = M \circ \hat{P} = I$), and we deduce $\Pi_S = I$ and the foregoing condition becomes

$$\hat{P} \circ \Delta_c [\Delta t] \circ M \cdot S(t) \approx \Delta_f [\Delta t] \cdot S(t). \quad (6)$$

And in the special case $O = R$, which we will also use, $R_R = I$, $R_S = M$, $P_R = I$, and $P_S = \hat{P}$, so equation (3) reverts to

$$\Delta_c [\Delta t] \cdot R(t) \approx M \circ \Delta_f [\Delta t] \circ \hat{P} \cdot R(t), \quad (7)$$

which is closely related to (1).

In all cases some measure of difference or distance is required to define approximation \approx ; such a measure may operate directly on microstates s , r , o , or on probability distribution state vectors S , R , O over these microstates as we assume below. Particular definitions of \approx will be made in section 3.3 (for $O = R$) and appendix (for $O = S$). The foregoing considerations apply to any dynamical system including stochastic, deterministic, and mixed stochastic/deterministic ones.

2.2. Fine- and coarse-scale dynamics

To apply the foregoing framework we need to define fine scale dynamics, coarse scale dynamics, observables, mappings between them, and a sense of approximation (\approx in figure 1). As in equation (7) above, we will report on the results of taking $O = R$. The approximation metrics will be defined in section 3.3. We now define fine and coarse scale models.

For a master equation derived from a large fine-scale reaction network (whether rule-based or not) we seek reduced coarse-scale models in the form of a Boltzmann distribution over states at each time point, with successive time points linked by an artificial and approximating dynamics on the ‘coupling constant’ or interaction parameters (now time-varying rather than constant) appearing in the Boltzmann energy function formula. In machine learning terms, our prolongation map \hat{P} is given at each instant in time by a probability distribution on fine-scale variables specified by a Markov random field (MRF) [11]. The MRF comprises a set of ‘clique potentials’ or ‘interaction potentials’. Each interaction potential is a function, usually a

monomial or polynomial, of just a few random variables. Each such potential function is multiplied by a scalar interaction potential strength, which we will call an ‘interaction parameter’. The sum of all the potentials (including their interaction parameter multiplicative factors) yields the energy function in the Boltzmann distribution. Unlike the potentials, the energy function depends on all the random variables. The way we apply this standard apparatus is as follows: the MRF random variables are interpreted as the fine-scale variables, and the MRF interaction parameters are taken to be the coarse-scale model dynamical variables. Only these interaction parameters can vary with time, and in our model they will vary continuously in time. Otherwise, the structure of each interaction potential is fixed and independent of time. Thus, the energy function and the MRF model depend on time only through the interaction parameters which are the coarse-scale dynamical variables.

Without the constraint between successive time points enforced by coarse-scale dynamics on the interaction parameters, the classic Boltzmann machine learning algorithm (BMLA) [12] can be used separately at each time point to optimize these unknown interaction parameters to fit samples drawn from many simulations of the full model. This learning algorithm optimizes the K–L divergence or relative entropy between sampled and modeled distributions, thereby defining a sense for the approximation relationship in section 2.1, but only for one instant in time. We slightly generalize the BMLA learning algorithm so that it allows for weight-sharing (components of the μ interaction parameter vector that are constrained eg. to be equal) and for polynomial interaction potentials of degree higher than two.

Coupling many such interaction-parameter inference problems together by insisting that the inferred interaction parameters μ all evolve according to imposed ordinary differential equation (ODE) dynamics, with a further set of learnable model-specifying meta-parameters θ defined in section 2.3 below, results in the graph constrained correlation dynamics (GCCD) method presented here and in [13].

A large space of stochastic dynamical systems ($S, \Delta_f[\Delta t]$) which can specialize to deterministic ones is specified by the master equation governing (possibly singular) probability distributions $p(s, t)$:

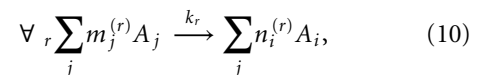
$$\frac{dp(t)}{dt} = W \cdot p(t), \quad (8)$$

where W is some linear operator acting on the state space of all distributions p over S and obeying conservation of probability, $\mathbf{1} \cdot W = 0$. Even though the master equation is linear, its effect on moments such as $\langle s_i \rangle_p(t)$ may be highly nonlinear.

For stochastic chemical kinetics the master equation specializes to the CME which can be written:

$$\begin{aligned} & \frac{d}{dt} p([n_i], t) \\ &= \sum_r k_r \left[\left(\prod_j (n_j - S_j^{(r)})_{m_j^{(r)}} \right) \right. \\ & \quad \times p([n_i - S_i^{(r)}], t) \\ & \quad \left. - \left(\prod_j (n_j)_{m_j^{(r)}} \right) p([n_i], t) \right], \quad (9) \end{aligned}$$

where $[n_i]$ is the vector of numbers n_i of molecules of each type i ; also in each reaction r , the stoichiometry of the reaction is defined by the following integers: $m_j^{(r)}$ copies of molecule j are destroyed and $n_j^{(r)}$ are created resulting in a net change of $S_j^{(r)} = n_j^{(r)} - m_j^{(r)}$ in the number of molecules of type j ; also the notation $(n)_m$ means the falling factorial $n!/(n-m)!$, and k_r is the reaction rate for reaction number r . This fully defines the fine-scale stochastic system for a mass-action chemical reaction network. Using the same notation, the chemical reaction network itself may be expressed as:



where A_i represents reacting chemical species number i and the sums are to be interpreted chemically rather than mathematically.

The Plenum implementation of dynamical grammars [2, 4] and the MCell Monte Carlo simulation software [3] can be used to express rule-based models and thereby to concisely define combinatorially many elementary reactants and reactions for molecular complexes such as CamKII (which will be introduced in section 3.1 below) and to efficiently simulate them. In addition, spatial diffusion processes can be added. Plenum uses computer algebra to express high-level biological models including those in which the number of compartments varies dynamically and hybrid stochastic/ODE systems. MCell has strong stochastic spatial capabilities and has been used extensively for synapse and neuronal simulations.

For coarse-scale approximate models, if we assume that the state space of the reduced model can be described as the product of state spaces for a fixed set of variables $r = \{\mu_\alpha\}$, then we may consider coarse-scale dynamical systems that through prolongation \hat{P} induce an instantaneous fine-scale probability distribution $\tilde{p}(s, t)$ defined by some Boltzmann distribution

$$\tilde{p}(s|t, \mu) = \exp \left[- \sum_\alpha \mu_\alpha(t) V_\alpha(s) \right] / Z(\mu(t)), \quad (11)$$

where $Z(\mu)$ normalizes \tilde{p} . This formula separates the time-evolution (which can only affect interaction parameters μ_α) from the correlation-controlling structure of interactions V_α . If there are as many values of α as elements in the full state space of s , then any

distribution can be described, but generally we choose a far sparser set of interaction terms. In general equation (11) has nonzero moments of all orders, though only a few moments $-\partial \log Z[\mu]/\partial \mu_k = \langle V_\alpha(s) \rangle$ can be controlled independently by varying the μ_k interaction parameters. This control would be exercised e.g. when one derives equation (11) by maximizing entropy subject to equality constraints on these moments $\langle V_\alpha(s) \rangle$ and on total probability. All other moments (which effectively have $\mu_\alpha = 0$) would fall where they may, following the principle of constrained maximum entropy obeyed by the Boltzmann distribution.

The essential information about the coarse-scale dynamics is contained in equation (11) above and equation (12) in section 2.3 below. In this setting, prolongation \hat{P} from coarse to fine is obtained by sampling from the Boltzmann distribution $\tilde{p}(r|t, \mu)$. The model reduction map M will be defined by statistical inference, from a sample of S to μ . Unlike the time-evolution maps $\Delta_f[\Delta t]$ and $\Delta_c[\Delta t]$, neither M nor \hat{P} must necessarily be linear on distributions, and in the special case of optimization algorithms such as maximum likelihood inference, maximum *a posteriori* inference, and BMLA, M would be nonlinear due to its optimization of an objective function that is not quadratic in both p and \tilde{p} . In sections 2.3 and 3 we will specialize and then apply the theory to stochastic biochemical networks.

2.3. Basis functions, smoothing, test cases

To define the coarse-scale stochastic model in terms of the time-evolving Boltzmann distribution of equation (11), we hypothesize that even though any particular sample of the stochastic nonlinear system will in general undergo discontinuous evolution, the probability distribution governing the ensemble of such samples are likely to evolve continuously in time (as does the master equation itself) even when projected down to distributions described by the statistical interaction parameters μ . We therefore further hypothesize continuous and deterministic ODE dynamics for the $\mu(t)$ interaction parameters:

$$\frac{d}{dt} \mu_\alpha(t) = f_\alpha(\mu(t)) = \sum_A \theta_{\alpha A} f_A(\mu(t)), \quad (12)$$

which is linear in new trainable model meta-parameters $\theta_{\alpha A}$ (referred to below as ‘model parameters’, and which must be distinguished from the interaction parameters μ) that are constant in time, unlike the time-varying interaction parameters μ . For basis functions $f_{\alpha A}(\mu)$ we use bases that arose in elementary solvable examples (two- and four-state binding models mentioned at the end of this subsection and described in [13]):

$$f_A(\mu) \in \bigcup_{\alpha, \beta} \left\{ 1, e^{\mu_\alpha}, e^{-\mu_\alpha}, \mu_\alpha^k, \right. \\ \left. \times \frac{1}{(\mu_\alpha + 1)}, e^{(\mu_\alpha - c)^2/2}, \right. \\ \left. \mu_\alpha \mu_\beta, e^{2(\mu_\alpha - \mu_\beta)^2}, e^{2(\mu_\alpha + \mu_\beta)^2} \right\}, \quad (13)$$

for $k \in \{1, \dots, 5\}$ and $c \in \{-3, \dots, +3\}$. Machine learning model selection algorithms (such as the ‘lasso’ algorithm of section 3.3 below) can be used to encourage sparsity in the use of bases i.e. in the matrix θ , which in turn favors good generalization performance. Many other forms for trainable ODE dynamics could be used in this ‘system identification’ subproblem, such as (nonlinear in θ) neural networks.

Like the Markovian equation (8), the deterministic equation (12) is differential in time so that the evolution of the coarse scale dynamical interaction parameters μ depends only on their state at the current time and not directly on their state at earlier times. However as remarked in [14], many consistent non-Markovian stochastic processes can be obtained from Markovian ones by integrating out extra degrees of freedom not otherwise needed. Similar phenomena obtain for differential equations. In GCCD it may be possible to do this by adding extra ‘hidden’ interaction parameters and/or extra random variables to the GCCD graph.

As a postprocessing step, the BMLA-learned trajectories of $\mu_k(t)$ interaction parameters could be smoothed in time t by convolution with a Gaussian in t and then differentiated with respect to time to get $d\mu/dt$; what we actually do is the mathematically equivalent operation of convolving with the analytic derivative of a Gaussian.

The solvable examples used to derive the basis functions in equation (13) were: (1) a two-state binding site model in which ligand binds to and unbinds from a site, and (2) a four-state, two-site cooperative binding model, both obeying detailed balance. The K–L divergence minimization algorithm derived in the appendix solved both of these problems correctly to high accuracy. Unfortunately, with these basis functions, the GCCD K–L divergence minimization algorithm exhibited numerical instability and failure to converge on the realistic CaMKII problem outlined below. It is possible that this problem could be solved by variations such as more extensive stacking (defined in the appendix), which would allow the use of more training data, or a different form for the ODEs such as different basis functions and/or ODEs nonlinear in θ . In particular the ODE right-hand sides could take the mathematical form of trainable nonlinear neural networks. Multilayer neural networks with a final linear layer would generalize equation (12) to include trainable basis functions. In section 3 below we report on the results of a different strategy, which is to optimize approximation in the $O=R$ or μ space (as in

equation (1) or (7)) rather than the $O = S$ space (as in equation (6)).

2.4. Previous work

If we multiply the appropriate master equation (equation (9) above) by monomials in key observables such as numbers of molecules of selected species in a chemical reaction network, and then sum over all states, we find ODEs for the time-evolution of various moments of the distribution over states. Unfortunately these equations do not *close*: the time derivative of lower-degree moments depends on the present value of higher-degree moments recursively, generating a countable infinity of coupled differential equations.

The goal of ‘moment closure’ methods [15–27] is to obtain explicit though approximate dynamics for some finite subset of the first-order moments $C_i = \langle s_i \rangle_{p(t)}$, the second-order moments $C_{ij} = \langle s_i s_j \rangle_{p(t)}$, and higher moments $C_{i_1 \dots i_k}^k = \langle s_{i_1} \dots s_{i_k} \rangle_{p(t)}$ of a collection of random variables s_i under some dynamics of their joint probability distribution $p(\vec{s}, t)$. Many approximate moment closure schemes have been developed starting from $k = 1$ mean field theory (systematically replacing $\langle s_i s_j \rangle_{p(t)}$ with a function $\langle s_i \rangle_{p(t)} \langle s_j \rangle_{p(t)}$ of the first-order moments as would be correct for independent distributions) from which one recovers ordinary deterministic chemical kinetics, and escalating to second-order ($k = 2$) moment closures that consistently keep track only of means and variances (as would be correct for a Gaussian joint distribution) in chemical reaction networks [15, 16], or in population biology reaction-diffusion models [17] explicitly, or by means of the Fokker–Planck equation [18] or stochastic differential equations such as the chemical Langevin equation [19] which may sometimes be further reduced [20].

A slightly higher order scheme is the Kirkwood superposition approximation that retains $\langle s_i s_j \rangle_{p(t)}$ ($k = 2$) but approximates triple correlations ($k = 3$) by a function of second-order correlations, is derivable from [22, 22] a constrained maximum-entropy sense of approximation \approx , and has been used in multicellular stochastic modeling [23]. Fully dynamic higher order cutoffs to the moment hierarchy for $k > 2$ include setting higher cumulants to zero [24], dropping higher order terms from the Kramers–Moyal expansion [25] using moment closure functions that would be correct for log-normal rather than Gaussian distributions [26], and ‘equation-free’ moment closure [27] by sparingly invoking fine-scale simulations.

Each of these moment closure methods has the character, when compared to a sampling algorithm, of first exponentially expanding the space in which dynamics are formulated using the master equation, and then trying to cut the exponentially large space back down to size. Typical results start from a small

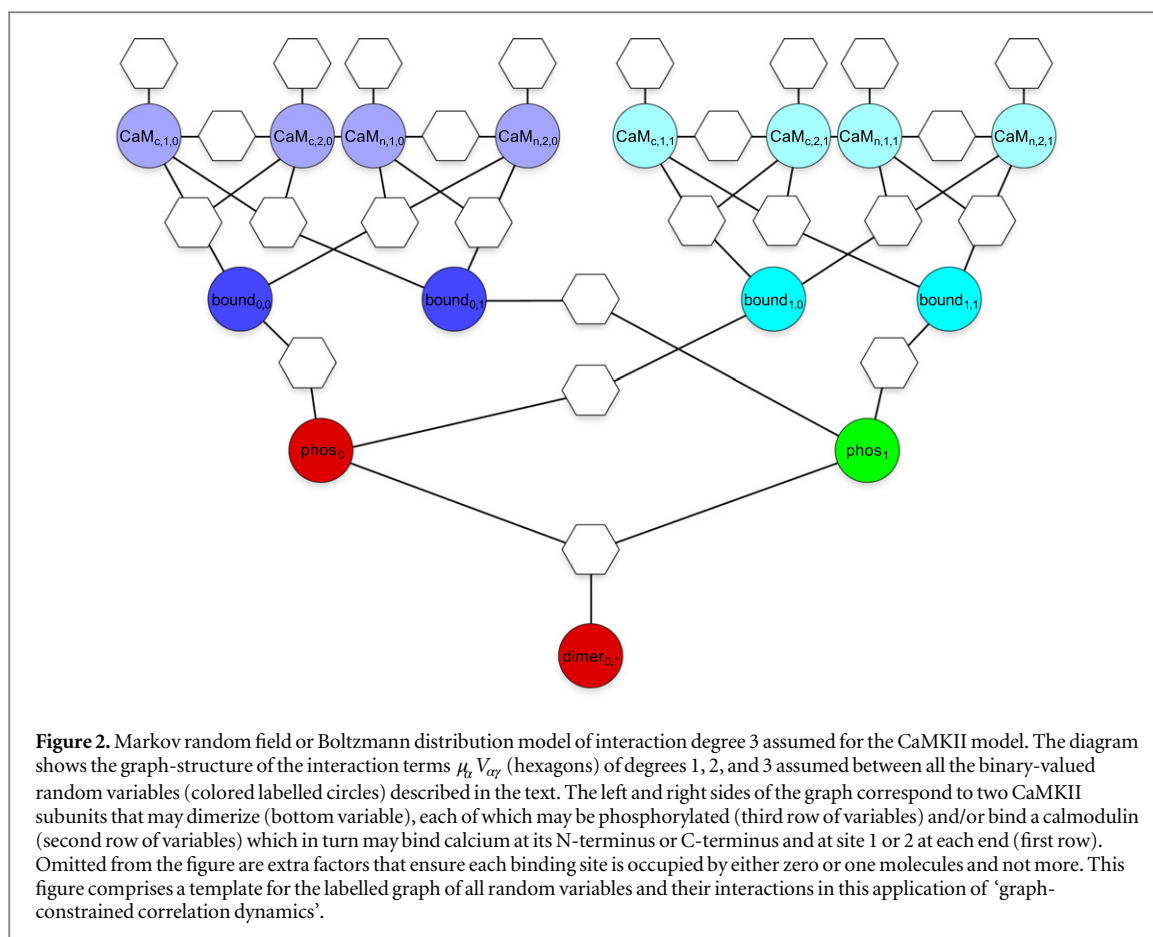
reaction network with $n < 10$ molecular species (and thus chemical/biological degrees of freedom if there is a single well-stirred compartment), and produce a more efficient algorithm for determining low-order moment trajectories for a possibly reduced model of between about $n/2$ and n molecular species, yielding model size reductions on the order of a factor of 1 to 2. The initial combinatorial explosion is not fully mitigated. This is an unpromising route if the goal is to find a large model reduction beyond what one already had at the fine scale (though not an impossible one, due to the need to run sampling simulations many times). We are proposing a different strategy for moment closure which more naturally results in model reduction with fewer chemical/biological degrees of freedom. From the moment closure point of view, what we are proposing is an arbitrary-order method particularly suited to approximating the CME and possibly related master equations, by a time-dependent variant of a Boltzmann distribution.

Additional model reductions for stochastic chemical kinetics, other than moment closure methods, include the classic strategy of using separation of time scales to eliminate fast degrees of freedom as carried out in e.g. the quasi-steady state approximation [28], in adiabatic course-graining [29], and with power law scaling of time with respect to an overall problem size parameter, differentially for different subsets of molecular species [30]. Another strategy for molecular species with small expected population sizes is the Finite State Projection method which proposes an adaptive truncation of the state space followed by analytic solution or bounding of the (exponentially big, were it not truncated) master equation [31]. Other reaction network model reduction methods are restricted to deterministic models [32, 33] including a reduction from 42 to 29 molecular species [34]. The most comparable method in terms of problem size may be [35] which like GCCD applies to rule-based reaction networks. We will quantitatively compare degrees of model reduction of these methods to GCCD in section 3.4.

As in the case of moment closure methods, all of these methods have advantages and interesting ideas but none that we know of are as yet in the same class of radical model size reduction as GCCD, in terms of fraction of molecular species retained after reduction, in a stochastic biochemical network model.

3. Computational experiments

Molecular complexes in general, and signal transduction complexes in particular often have state space explosions that pose problems for simulation and modeling. One such macromolecular complex is Ca^{2+} /calmodulin-dependent protein kinase II (CaMKII) in synapses, which is activated when it binds to multiple calmodulin (CaM) molecules that in turn



bind to multiple calcium ions. These processes trigger a cascade of reactions in a signal transduction pathway following Ca^{2+} influx in response to activation of ligand-gated NMDARs, supporting memory formation and learning.

We applied GCCD to this system as modeled by [1] and as simulated by the Plenum implementation of dynamical grammars [2, 4] and also in a much larger spatial simulation using MCell [3].

3.1. CaMKII system

The synaptic signal transduction pathway that starts with calcium ion (Ca^{2+}) influx through voltage-dependent calcium channels and NMDARs leads ultimately to functional consequences including long-term potentiation (LTP), long-term depression, and spike-timing dependent plasticity underlying learning and memory formation in the hippocampus. The pathway as studied and modeled in [1] is structurally a bit involved. It begins with an externally imposed influx of calcium ion Ca^{2+} . Calcium ions bind to the calmodulin protein (CaM), which has four calcium-binding sites, two at the N-terminal end and two at the C-terminal end. CaM in any state of calcium-loading can then bind to unphosphorylated CaMKII monomer (which has one phosphorylation site relevant for activation). However, the binding and unbinding rates for calcium ion to CaM depends on the state of the

other binding sites of the CaM protein, and also on whether or not that CaM is bound to CaMKII. Likewise the binding and unbinding rates for CaM to unphosphorylated CaMKII monomer depend on the state of CaM. Two CaMKII monomers, each loaded with CaM in any calcium-binding state, but at most one of which is phosphorylated, may then dimerize (again with state-dependent rates). Dimers may phosphorylate one of their constituent subunits and promptly dissociate; autophosphorylated monomer CaMKII is taken to be the pathway output. Our goal is to produce a reduced stochastic model simplifying the structure of this fine-scale model as formulated in the MCell and Plenum models (model files in supplementary information) that aim to implement stochastic versions of the reaction network of [1].

Many subsequent stages of the biological pathway are thereby omitted, notably the formation of a CaMKII holoenzyme comprising a ring of six dimers in dodecameric complex. This holoenzyme structure implies an even greater combinatorial explosion of states that poses a future modeling challenge, that may best be met by aggressive model reduction methods such as the GCCD method proposed here. Further downstream components of the pathway beyond CaM and the CaMKII holoenzyme are outlined in [8]. However we leave such explorations, which could aim to extract novel biological consequences from

combinatorially large stochastic reaction network models of the NMDA receptor pathway by applying the GCCD model reduction technique, to future research.

3.2. Boltzmann machine preprocessing step

Figure 2 shows part of the assumed Boltzmann distribution model interaction graph, or MRF, of binary-valued random variables (circles) and monomial interaction potentials of degree 1, 2, and 3 (hexagons). The first row of variables represent the binding of calcium to calmodulin (CaM). With subscripts these ± 1 -valued random variables are labelled ‘CaM_{c/n,a,i}’. They are indexed by the C-terminus versus the N-terminus of the calmodulin protein (*c* or *n*), the numerical index of the binding site on that end (*a* = 1 or 2), and the numerical index *i* (*i* = 0 or 1 illustrated; *i* ∈ {0, 1, 2} used in Plenum simulations below) of a calmodulin molecule which may bind to a CaMKII subunit (indexed by *j* = 0 or 1 illustrated; *j* ∈ {0, ... 8} used in Plenum simulations below). The second row of variables ‘bound_{i,j}’ records the state of binding of CaM to CaMKII subunits. The third row of variables ‘phos_j’, also written (in the notation of the MCell model) as ‘Kkp_j’, records the binary phosphorylation state of each CaMKII subunit, and the fourth row of variables ‘dimer_{j,j'}’ records whether or not two such subunits dimerize. Not shown are additional cardinality-fixing or winner-take-all interactions enforcing the constraints that (if it occurs) binding is an exclusive relationship between CaM molecules and CaMKII subunits, and likewise for dimerization between two CaMKII subunits.

Weight-sharing is an important strategy in machine learning, widely used to reduce the number of trainable parameters and thereby increase generalization power for a given amount of data. Our weight-sharing scheme shares interaction parameters μ_x within categories of monomial interactions that seem likely, according to testable human intuition, to have similar interaction strengths if trained separately on far more data. We now introduce some notation for the weight-sharing. Let $\mathcal{I} = \{0, \dots \#\text{CaM} - 1\}$ and $\mathcal{J} = \{0, \dots \#\text{CaMKIIsubunits} - 1\}$. We have the following categories of ± 1 -valued random variables s_i :

$$\begin{aligned} &\text{CaM}_{c/n,a,i} \quad (\forall c/n \in \{c, n\}) \\ &\quad (\forall a \in \{1, 2\})(\forall i \in \mathcal{I}), \\ &\text{bound}_{i,j} \quad (\forall i \in \mathcal{I})(\forall j \in \mathcal{J}), \\ &\text{Kkp}_j \quad (\forall j \in \mathcal{J}), \\ &\text{dimer}_{j,j'} \quad (\forall j < j' | j, j' \in \mathcal{J}). \end{aligned}$$

We have used the following eight categories of monomial interactions s_i , $s_i s_j$, or $s_i s_j s_k$ (all taking values in $\{\pm 1\}$):

$$\begin{aligned} &\text{CaM}_{c,a,i} \quad (\forall a \in \{1, 2\})(\forall i \in \mathcal{I}), \\ &\text{CaM}_{n,a,i} \quad (\forall a \in \{1, 2\})(\forall i \in \mathcal{I}), \\ &\text{CaM}_{c,1,i} \text{CaM}_{c,2,i} \quad (\forall i \in \mathcal{I}), \\ &\text{CaM}_{n,1,i} \text{CaM}_{n,2,i} \quad (\forall i \in \mathcal{I}), \\ &\text{bound}_{i,j} \text{CaM}_{c,1,i} \text{CaM}_{c,2,i} \quad (\forall i \in \mathcal{I})(\forall j \in \mathcal{J}), \\ &\text{bound}_{i,j} \text{CaM}_{n,1,i} \text{CaM}_{n,2,i} \quad (\forall i \in \mathcal{I})(\forall j \in \mathcal{J}), \\ &\text{Kkp}_j \text{bound}_{i,j} \quad (\forall i \in \mathcal{I})(\forall j \in \mathcal{J}), \\ &\text{Kkp}_j \text{Kkp}_{j'} \text{dimer}_{j,j'} \quad (\forall j < j' | j, j' \in \mathcal{J}). \end{aligned}$$

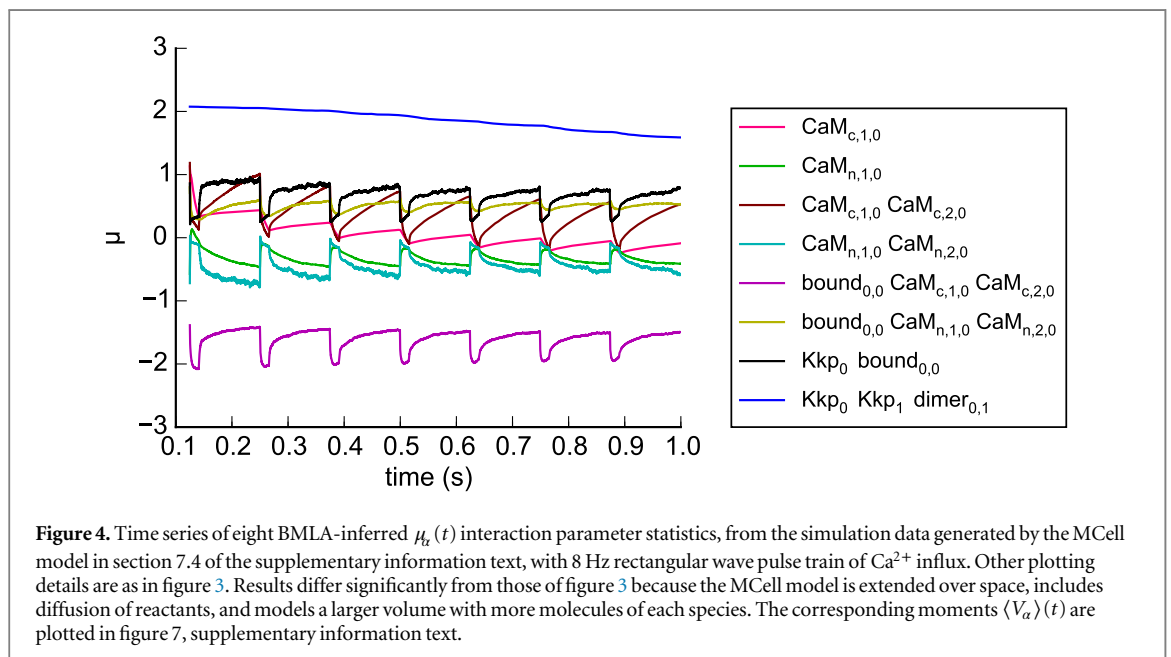
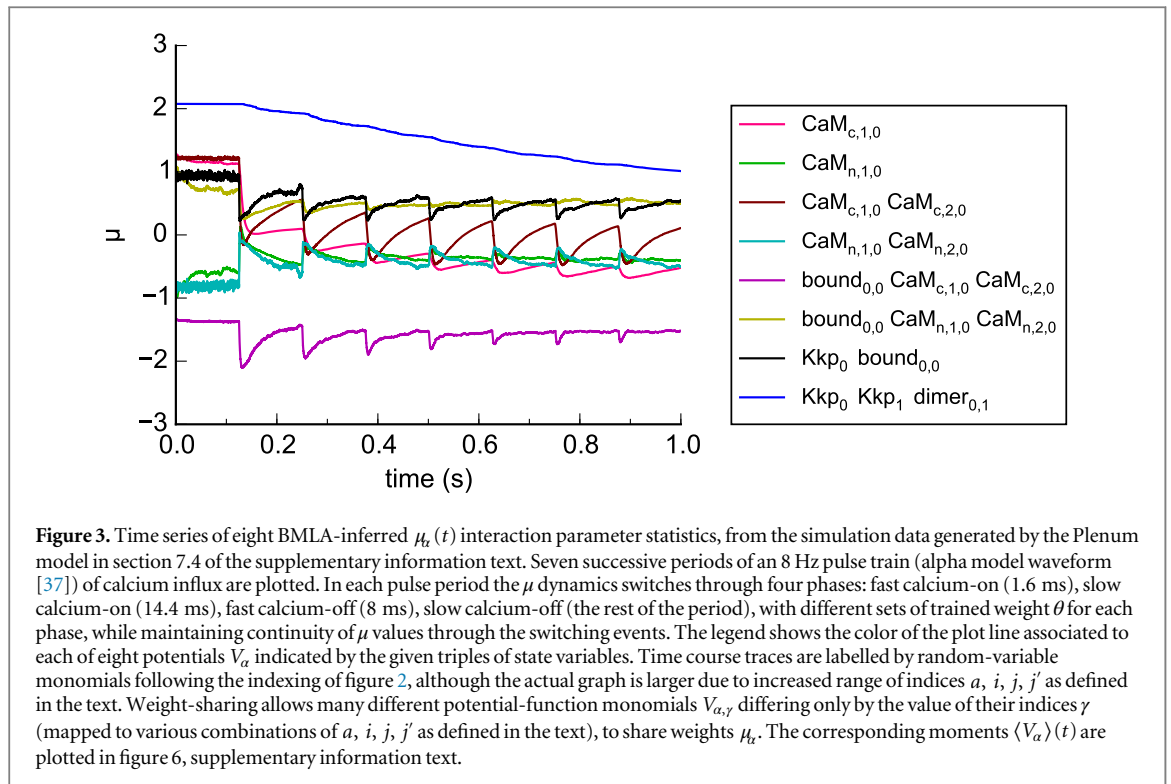
We number these weight-sharing categories $\alpha \in \{1, \dots 8\}$. Different categories α have different numbers n_α of monomial interactions depending on which bound indices *a*, *i*, *j*, *j'* they run over. We take the potential function V_α for each category to be the category-average of the constituent monomials $V_{\alpha,\gamma} = s_i s_j s_k$, or $s_i s_j s_k$ given above, so that $V_\alpha = (1/n_\alpha) \sum_{\gamma=1}^{n_\alpha} V_{\alpha,\gamma}$.

The resulting Boltzmann distribution can be sampled by standard Monte Carlo methods such as Metropolis–Hastings or Gibbs sampling. We use the ‘Dependency Diagrams’ software [13] (availability described in supplementary information) to do this. A crucial wrinkle on our use of such sampling algorithms is that we have two different biological conditions under which they get used: external calcium influx can be ‘on’ or ‘off’. We train four different sets of coarse-scale dynamical model parameters θ as described in section 3.3 below, for four phases (early and late phases for calcium influx on and for calcium influx off), and for pulsatile or periodic calcium influx we cycle through the four trained (or partly trained) models, while preserving the interaction parameters μ through each instantaneous phase-switching event. Once trained, these four models predict dynamical responses to any other temporal pattern of calcium influx switching including the use of periodic switching with frequencies not in the training set.

A logical alternative to this procedure would be to use just two phases for calcium on and off, and to add the binary calcium-influx variable into the GCCD graph of figure 2 with suitable connections to allow the switch variable to join in modulating some or all of the potentials V_α . However, we were not able to get this somewhat cleaner approach to work numerically. Just switching between two phases (Ca²⁺ influx on versus off) rather than four phases without modifying the GCCD graph also produced less robust behavior.

For the MCell simulations below the waveform for calcium influx was a pulse train or rectangular wave, with the ‘on’ duration being 16 ms. For the Plenum simulations we used the ‘alpha model’ theoretical calcium influx profile [37].

In figures 3 and 4, the inferred trajectories of μ time-varying interaction parameters are shown for the non-spatial Plenum [2] model (figure 3) and the spatial MCell [3] model (figure 4). The corresponding moments $\langle V_\alpha \rangle \in [-1, 1]$ are shown in figures 6 and 7



of the supplementary information, where their relation to concentrations is discussed. From figures 3 and 4 it is evident that the inferred μ_x interaction parameter trajectories are remarkably continuous in time, empirically justifying the assumption of ODE dynamics in equation (12).

3.3. GCCD

The resulting time series (such as figures 3 and 4) are convolved with the analytic temporal derivative of a Gaussian filter in order to smoothly estimate the rates of change $d\mu_x/dt$ of the interaction parameters $\mu_x(t)$.

Such temporal smoothing is useful since taking derivatives of a noisy time series tends to enhance the noise, and in the absence of smoothing that occurs for our time series [13]. The resulting smoothed time derivatives are fit to equation (12) using either (1) online minimization of the K–L divergence as outlined in appendix for which $O = S$, or (2) lasso-regularized linear regression [36] for which $O = R$, and which performs model selection on the bases of equation (13) as discussed there. Here we report numerical results for the second method, which also defines a meaning for the \approx symbol in section 2.1 as the lasso-regularized

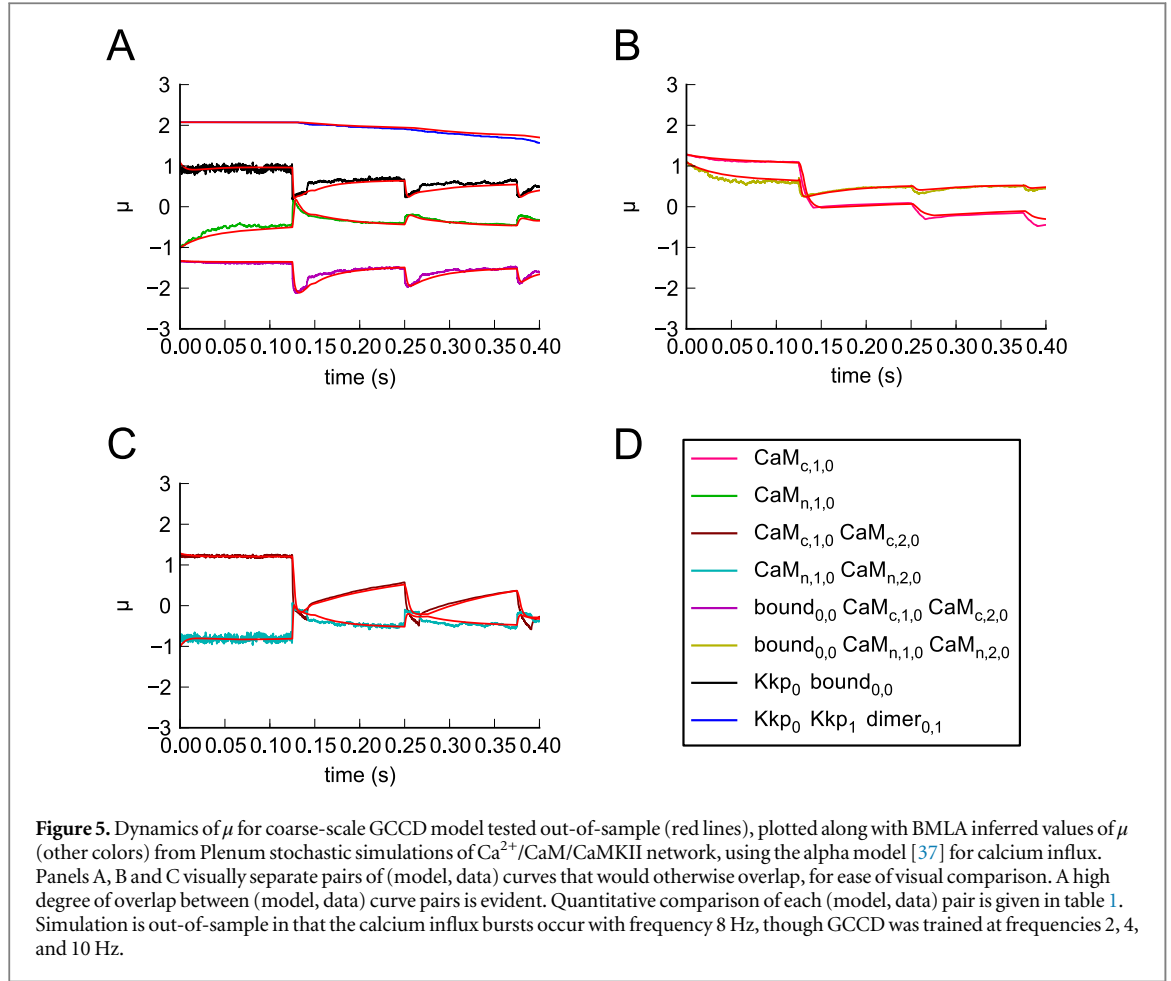


Figure 5. Dynamics of μ for coarse-scale GCCD model tested out-of-sample (red lines), plotted along with BMLA inferred values of μ (other colors) from Plenum stochastic simulations of $\text{Ca}^{2+}/\text{CaM}/\text{CaMKII}$ network, using the alpha model [37] for calcium influx. Panels A, B and C visually separate pairs of (model, data) curves that would otherwise overlap, for ease of visual comparison. A high degree of overlap between (model, data) curve pairs is evident. Quantitative comparison of each (model, data) pair is given in table 1. Simulation is out-of-sample in that the calcium influx bursts occur with frequency 8 Hz, though GCCD was trained at frequencies 2, 4, and 10 Hz.

(L_1 -regularized) sum of squared differences for the time derivatives of the $\mu_\alpha(t)$ statistical interaction parameters (summed over α , discretized t , and over any set of initial conditions and/or other input conditions c such as calcium influx frequency). Thus, we optimize the model parameters $\theta_{\alpha A}$ by minimizing the score

$$S([\theta_{\alpha A}]) = \sum_{\alpha, t_{\text{discr}}, c} \left\| \left. \frac{d\mu_\alpha(t)}{dt} \right|_{\text{fit}} [\theta_{\alpha A}] - \left. \frac{d\mu_\alpha(t)}{dt} \right|_{\text{BMLA}} \right\|^2 + \lambda \sum_{\alpha A} |\theta_{\alpha A}|. \quad (14)$$

(Defining a sense of approximation \approx as needed in section 2.1) which by equation (12) is equivalent to

$$S([\theta_{\alpha A}]) = \sum_{\alpha, t_{\text{discr}}, c} \left\| \left. \frac{d\mu_\alpha(t)}{dt} \right|_{\text{BMLA}} - \sum_A \theta_{\alpha A} f_A(\mu) \right\|^2 + \lambda \sum_{\alpha A} |\theta_{\alpha A}|, \quad (15)$$

a form that is explicitly lasso-regularized least squares optimization of the trainable interaction parameters θ . The single scalar hyperparameter λ was set using leave-one-out cross validation, with each calcium influx spike held out in turn. 150 out of 253 model bases parameters were always rejected by the lasso

Table 1. Normalized rms errors in figure 5.

Interaction parameter	rms error	Normalized rms error
CaM($c,1,0$)	rms1 = 0.062	cvrms1 = 0.132
CaM($n,1,0$)	rms2 = 0.070	cvrms2 = 0.174
CaM($c,1,0$) CaM($c,2,0$)	rms3 = 0.096	cvrms3 = 0.170
CaM($n,1,0$) CaM($n,2,0$)	rms4 = 0.075	cvrms4 = 0.141
bound($0,0$) CaM($c,1,0$) CaM($c,2,0$)	rms5 = 0.068	cvrms5 = 0.044
bound($0,0$) CaM($n,1,0$) CaM($n,2,0$)	rms6 = 0.061	cvrms6 = 0.118
Kkp0 bound($0,0$)	rms7 = 0.090	cvrms7 = 0.133
Kkp0 Kkp1 dimer($0,1$)	rms8 = 0.044	cvrms8 = 0.023

algorithm, and the remaining 103 bases were used sparsely depending on the μ_α derivative being fit, which of the four phases was being fit, and which BMLA experiment data set was being used.

The resulting constrained time-evolution of ODE-constrained interaction parameters $\mu_\alpha(t)$ evaluated out-of-sample (i.e. using different data than was used for training the model parameters) was almost indistinguishable from the unconstrained values of optimal interaction parameters obtained by BMLA, as a function of time over several calcium influx cycles, as shown in figure 5.

Numerical errors in figure 5 are shown in table 1, computed as root mean squared (rms) error and also as normalized rms error, in which the normalization is done by finding the average of the absolute value of each target BMLA time course, and dividing both the target and corresponding prediction time course by this average absolute value before computing the rms error as usual.

The results show good out-of-sample quantitative agreement for all eight time series.

3.4. Discussion of results

In quantitative terms, the degree of model reduction obtained by GCCD in the CaMKII example is large. Eight dynamical variables (the interaction parameters μ) suffice to predict key outputs such as the global degree of CaMKII phosphorylation, each of which can be computed from expectations of random variables s in the Boltzmann distribution of equation (11). But the fine-scale set of dynamical variables is much larger. In the MCell simulations we may conservatively count it as the integer-valued populations of the following classes of molecular species: free Ca^{2+} , free CaM ($3 \times 3 + 1 = 10$ species), monomeric CaMKII subunit which can bind CaM in any of its states and can also be phosphorylated ($3 \times 3 \times 2 = 18$ species), and dimerize if at most one subunit is phosphorylated ($9 \times 9 + 9 \times 10/2 = 126$ species; phosphorylated dimers dissociate before they can doubly phosphorylate) for a total of 155 species each of which has a dynamical random variable, and therefore a total reduction from 155 to just eight dynamical variables, which is very large.

In one sense this reduction in the number of dynamical variables strongly understates the situation, because in the actual MCell simulation (though not in the Plenum simulations), every individual chemical species has its own independent three-dimensional position which is also a dynamical random variable. Given that a typical molecular population excluding Ca^{2+} is $145 \text{ CaM} + 385 \text{ CaMK} = 530$, and including each 24-unit Ca^{2+} pulse is still greater, and that the number of position degrees of freedom is three times greater (1590 or more), the reduction to just eight dynamical variables μ_1 through μ_8 as listed in figures 3–5 is even more remarkable.

Comparable figures for the (deliberately non-spatial and well-mixed) Plenum simulations are again 155 molecular species reduced down to eight. An intermediate step is the formulation of the graph in figure 2 which has just eight interaction parameters (associated with the hexagonal interaction nodes) due to weight sharing, but it has many more molecular binding variables (circular nodes in figure 2). For the Plenum model we can count these variables as follows: due to the smaller simulated volume than for the MCell model, the index i for CaM and the index j for CaMKII run from 0 to 2 and 0 to 8 respectively. If we

replicate the circular nodes in the graph of figure 2 accordingly, there are 4×3 , 3×9 , 9, and $9 \times 10/2$ variables respectively in rows 1–4 of the full version of the graph illustrated in figure 5, for a total of 93 fine-scale binary-valued variables in a highly structured pattern.

As stated in section 2.4, most current results for stochastic model reduction start from a small reaction network with handful of chemical species, and produce a more efficient (sometimes much more efficient) modeling algorithm for a possibly reduced model with model size reductions on the order of a factor of 1 to 2. The authors of [35], a stochastic and rule-based model reduction method as is GCCD, achieve a larger model reduction in an EGF signal transduction model from 2768 to 609 molecular species, for a $4.5 \times$ reduction factor or a 0.81-power relation of reduced to full model ($609 \simeq 2768^{0.809}$). We have demonstrated for GCCD at least 155 to 8 for a $19.5 \times$ reduction factor, or a 0.41-power relation ($8 \simeq 155^{0.412}$). This factor of almost 20 breaks decisively out of the pattern of model size reductions on the order of a factor of just 1 to 2 in number of chemical or biological degrees of freedom. Exploring tradeoffs between accuracy of approximation and amount of model size reduction (whether measured in direct ratios, or powers, of number of degrees of freedom before and after reduction) for increasingly large models would therefore seem to be an attractive topic for future work.

To what features of GCCD or the present problem do we owe these very substantial reductions in model size? Future work could disentangle the following seemingly relevant factors: (1) GCCD can be applied to rule-based models, which are highly structured in that (as shown in the Plenum model code in the supplementary information text) a small number of rules can combinatorially code for a much larger molecular species-level reaction network. Thus an underlying simplicity is available. (2) The use of weight-sharing may make it possible to exploit such underlying simplicity in the problem domain. (3) The machine learning components of GCCD (BMLA and the new procedures for determining GCCD model parameters θ) generalize directly from specific simulation data rather than algebraically and in full generality from the mathematical form of the fine-scale model. So currently available computer power is used effectively. (4) The Boltzmann distribution is a natural form for prolongation from coarse to fine models since by constrained entropy maximization it doesn't add any more information than is given by constraints on whatever moments were chosen for use in the GCCD graph structure. (5) The graph structure of GCCD is a good mechanism for importing biological knowledge and expertise into the model reduction process.

4. Conclusion

We propose a nonlinear model reduction method particularly suited to approximating the CME for stochastic chemical reaction networks (including highly structured ones resulting from ‘parameterized’ or ‘rule-based’ reactions), by a time-dependent variant of a Boltzmann distribution. The resulting GCCD method can be an accurate nonlinear model reduction method for stochastic molecular reaction networks involving a combinatorial explosion of states, such as the CaMKII signal transduction complex that is essential to synaptic function, particularly in neuronal learning processes such as LTP. The GCCD method could be further developed in many directions, including application to model-reduction for the master equation semantics of more challenging molecular complexes such as the CaMKII dodecamer, use of the resulting reduced models to extract novel biologically relevant predictions, and generalizing the method to yet more general reaction-like biological modeling formalisms capable of expressing multiscale models in developmental biology [4].

Acknowledgments

We wish to acknowledge many useful discussions with M Kennedy, S Pepke, Tamara Kinzer-Ursem, and D H Sharp. This work was supported by NIH grant RO1 GM086883 and also supported in part by the United States Air Force under Contract No. FA8750-14-C-0011 under the DARPA PPAML program, by NIH grant R01 HD073179 to Ken Cho and EM, by the Leverhulme Trust, and by the hospitality of the Sainsbury Laboratory Cambridge University. TB and TS were supported by NIH P41-GM103712 National Center for Multiscale Modeling of Biological Systems; NIH MHO79076, and the Howard Hughes Medical Institute.

Appendix A. Online learning derivations

We begin with the definition of KL divergence

$$D_{KL}(\tilde{p} \parallel p) = - \int \tilde{p} \log(p/\tilde{p}) dx \quad (16)$$

(or equivalently, $\int \tilde{p} \log(\tilde{p}/p)$). We could equally well begin with the divergence in the other direction, as $-\int p \log(\tilde{p}/p)$; the analogous derivation in that case is similar to what follows (and is performed in appendix A of [13]) but in our experience the resulting training algorithm produced slightly less reliable results.

Our approach will be to compute the derivative $\partial D_{KL}/\partial \mu_\alpha$, then take the time-derivative of this term, and minimize that. Minimization of $\partial D_{KL}/\partial \mu_\alpha$ corresponds to matching the distribution \tilde{p} to p at an initial time point, and we will need to take for granted the ability to do this well once, as an initialization. Then, if

we have done a good job of that, keeping the change in this term 0—setting the derivative of this term equal to zero and solving for the parameters of a GCCD model—will track the optimal solution as the two distributions change in time.

Though we have so far defined variable x to take values in a discrete space, we use the integral notation throughout this derivation, as integration specializes to summation on a discrete domain, but the converse is not true.

The first few steps here are just pulling apart terms, starting from the definitions of the MRF, as follows:

$$D_{KL}(\mu(t)) = - \int \tilde{p}(x; \mu(t)) \log \left(\frac{p(x; t)}{\tilde{p}(x; \mu(t))} \right) dx$$

so

$$D_{KL}(\mu(t)) = - \int \tilde{p}(x; \mu(t)) \times \left(\sum_{\beta=1}^{\text{cliques}} \mu_\beta(t) V_\beta(x) + \log(Z(\mu(t))) + \log(p(x; t)) \right) dx.$$

Now evaluate the derivative $\partial [D_{KL}(\mu(t))]/\partial \mu_\alpha$. Beginning with the product rule, we have

$$\begin{aligned} \frac{\partial D_{KL}(\mu(t))}{\partial \mu_\alpha} &= - \int \left(\frac{\partial}{\partial \mu_\alpha} \tilde{p}(x; \mu(t)) \right) \times \left(\sum_{\beta=1}^{\text{cliques}} \mu_\beta(t) V_\beta(x) + \log(Z(\mu(t))) + \log(p(x; t)) \right) dx \end{aligned} \quad (17)$$

$$- \int \tilde{p}(x; \mu(t)) \quad (18)$$

$$\times \frac{\partial}{\partial \mu_\alpha} \left(\sum_{\beta=1}^{\text{cliques}} \mu_\beta(t) V_\beta(x) + \log(Z(\mu(t))) + \log(p(x; t)) \right) dx. \quad (19)$$

Breaking this expression down, we begin by evaluating $\frac{\partial}{\partial \mu_\alpha} \tilde{p}(x; \mu(t))$.

$$\begin{aligned} \frac{\partial}{\partial \mu_\alpha} \tilde{p}(x; \mu(t)) &= \frac{\partial}{\partial \mu_\alpha} \frac{\prod_\beta e^{-\mu_\beta V_\beta(x)}}{Z(\mu(t))} \\ &= \tilde{p}(x) \left(\langle V_\alpha \rangle - V_\alpha(x) \right). \end{aligned} \quad (20)$$

Unless otherwise noted, all expectations $\langle \dots \rangle$ are with respect to the distribution \tilde{p} .

Plugging this result back into equation (19), and using $\partial \log(p(x; t))/\partial \mu_\alpha = 0$, along with the evaluation of $\partial \log(Z(\mu(t)))/\partial \mu_\alpha$ as $-\langle V_\alpha \rangle$, we have

$$\begin{aligned} & \frac{\partial \mathcal{D}_{KL}(\mu(t))}{\partial \mu_\alpha} \\ &= -\int \tilde{p}(x; \mu(t)) \left(\langle V_\alpha \rangle - V_\alpha(x) \right) \\ & \quad \times \left(\sum_{\beta=1}^{\text{cliques}} \mu_\beta(t) V_\beta(x) + \log(Z(\mu(t))) \right. \\ & \quad \left. + \log(p(x; t)) \right) dx \\ & \quad - \int \tilde{p}(x; \mu(t)) \\ & \quad \times \frac{\partial}{\partial \mu_\alpha} \left(\sum_{\beta=1}^{\text{cliques}} \mu_\beta(t) (V_\beta(x) - \langle V_\alpha \rangle) \right) dx. \end{aligned} \quad (21)$$

If we separate the second integral, we see that the two halves cancel:

$$\begin{aligned} & \int \tilde{p}(x; \mu(t)) (V_\alpha(x) - \langle V_\alpha \rangle) dx \\ &= \int \tilde{p}(x; \mu(t)) V_\alpha(x) dx - \int \tilde{p}(x; \mu(t)) \langle V_\alpha \rangle dx \\ &= \int \tilde{p}(x; \mu(t)) V_\alpha(x) dx - \langle V_\alpha \rangle \int \tilde{p}(x; \mu(t)) dx \\ &= \langle V_\alpha \rangle - \langle V_\alpha \rangle = 0. \end{aligned}$$

We can now absorb the leading minus sign, leaving

$$\begin{aligned} & \frac{\partial \mathcal{D}_{KL}(\mu(t))}{\partial \mu_\alpha} \\ &= \int \tilde{p}(x; \mu(t)) (V_\alpha(x) - \langle V_\alpha \rangle) \\ & \quad \times \left(\sum_{\beta=1}^{\text{cliques}} \mu_\beta(t) V_\beta(x) \right. \\ & \quad \left. + \log(Z(\mu(t))) + \log(p(x; t)) \right) dx. \end{aligned} \quad (22)$$

Now we wish to find the derivative of equation (22) with respect to time. In order to accomplish this, we first name pieces of equation (22). Let $A = \tilde{p}(x; \mu(t)) (V_\alpha(x) - \langle V_\alpha \rangle)$, $B = \sum_{\beta=1}^{\text{cliques}} \mu_\beta(t) V_\beta(x)$, $C = \log Z(\mu(t))$, $D = \log p(x; t)$. Then we can write the desired derivative as

$$\begin{aligned} \frac{d}{dt} \frac{\partial \mathcal{D}_{KL}(\mu(t))}{\partial \mu_\alpha} &= \int \left[A \frac{\partial}{\partial t} B + A \frac{\partial}{\partial t} C + A \frac{\partial}{\partial t} D \right. \\ & \quad \left. + (B + C + D) \frac{\partial}{\partial t} A \right] dx. \end{aligned} \quad (23)$$

Concentrating on the first two of these terms, $\int [A \partial/\partial t B + A \partial/\partial t C] dx$, we see that $\partial B/\partial t = \sum_{\beta} (\partial \mu_\beta / \partial t) V_\beta$ and, using the chain rule, $\partial C/\partial t = \sum_{\beta} (\partial \mu_\beta / \partial t) (\partial \log Z / \partial \mu_\beta)$. Thus,

$$\begin{aligned} & \int \left[A \frac{\partial}{\partial t} B + A \frac{\partial}{\partial t} C \right] dx \\ &= \int A \left[\sum_{\beta} \frac{\partial \mu_\beta}{\partial t} (V_\beta - \langle V_\beta \rangle) \right] dx \end{aligned}$$

$$\begin{aligned} &= \int \tilde{p}(x; \mu(t)) \sum_{\beta} \frac{\partial \mu_\beta}{\partial t} \\ & \quad \times (V_\beta - \langle V_\beta \rangle) (V_\alpha - \langle V_\alpha \rangle) dx. \end{aligned}$$

Shifting the integral inside the sum, we recognize the expression for the covariance between functions V_α and V_β , where $\langle (x - \langle x \rangle)(y - \langle y \rangle) \rangle = \text{Cov}(x, y) = \langle xy \rangle - \langle x \rangle \langle y \rangle$, so

$$\begin{aligned} & \int \left[A \frac{\partial}{\partial t} B + A \frac{\partial}{\partial t} C \right] dx \\ &= \sum_{\beta=1}^{\text{cliques}} \frac{\partial \mu_\beta(t)}{\partial t} \text{Cov}(V_\alpha, V_\beta) \\ &= \sum_{\beta=1}^{\text{cliques}} \frac{\partial \mu_\beta(t)}{\partial t} (\langle V_\beta V_\alpha \rangle - \langle V_\alpha \rangle \langle V_\beta \rangle). \end{aligned} \quad (24)$$

Turning our attention now to the fourth term of equation (23):

$$\begin{aligned} & \int \left(\frac{\partial}{\partial t} \left(\tilde{p}(x; \mu(t)) (V_\alpha(x) - \langle V_\alpha \rangle) \right) \right) \\ & \quad \times \left(\sum_{\beta=1}^{\text{cliques}} \mu_\beta(t) V_\beta(x) \right) \\ & \quad + \log(Z(\mu(t))) + \log(p(x; t)) \Big) dx, \end{aligned}$$

applying product and chain rules to equation (20), the time derivative of A , where

$$\partial/\partial t A = \partial \left[\tilde{p}(x; \mu(t)) (V_\alpha(x) - \langle V_\alpha \rangle) \right] / \partial t,$$

is

$$\begin{aligned} \frac{\partial}{\partial t} A &= \sum_{\beta} \left[\frac{\partial \mu_\beta}{\partial t} \tilde{p}(x) (\langle V_\beta \rangle - V_\beta(x)) \right. \\ & \quad \left. \times (V_\alpha(x) - \langle V_\alpha \rangle) \right] \\ & \quad - \tilde{p}(x; \mu(t)) \frac{\partial}{\partial t} \langle V_\alpha \rangle \\ &= -\tilde{p}(x; \mu(t)) \sum_{\beta} \frac{\partial \mu_\beta}{\partial t} (V_\beta(x) \\ & \quad - \langle V_\beta \rangle) (V_\alpha(x) - \langle V_\alpha \rangle) \\ & \quad + \tilde{p}(x; \mu(t)) \sum_{\beta} \frac{\partial \mu_\beta}{\partial t} (\langle V_\alpha V_\beta \rangle \\ & \quad - \langle V_\alpha \rangle \langle V_\beta \rangle). \end{aligned} \quad (25)$$

Note that the covariance between V_α and V_β has appeared again, and that it is being subtracted from terms which have the same form as the terms inside a covariance. That is, integrating over the first part of equation (25) would again produce the covariance between V_α and V_β , times the derivative of μ .

Terms such as $V_\beta(x) - \langle V_\beta \rangle$ recur regularly throughout this derivation. Therefore, we define a new

notation. Let $\Delta X \equiv X - \langle X \rangle$. Then we can rewrite the covariance in equation (24) as

$$\begin{aligned} & \sum_{\beta=1}^{\text{cliques}} \frac{\partial \mu_{\beta}(t)}{\partial t} \left(\langle V_{\beta} V_{\alpha} \rangle - \langle V_{\alpha} \rangle \langle V_{\beta} \rangle \right) \\ &= \sum_{\beta=1}^{\text{cliques}} \frac{\partial \mu_{\beta}(t)}{\partial t} \langle \Delta V_{\alpha} \Delta V_{\beta} \rangle. \end{aligned}$$

Additionally, equation (25) fits the same pattern, with

$$\begin{aligned} X &= \left(V_{\beta}(x) - \langle V_{\beta} \rangle \right) \left(V_{\alpha}(x) - \langle V_{\alpha} \rangle \right) \\ &= \left(\Delta V_{\alpha} \Delta V_{\beta} \right). \end{aligned}$$

So, we may rewrite this as

$$\frac{\partial}{\partial t} A = -\tilde{p}(x; \mu(t)) \sum_{\beta} \frac{\partial \mu_{\beta}}{\partial t} \Delta \left(\Delta V_{\alpha} \Delta V_{\beta} \right).$$

Plugging this in and copying the definitions for B , C , and D , we have

$$\begin{aligned} & \int (B + C + D) \frac{\partial}{\partial t} A dx \\ &= - \int \tilde{p}(x; \mu(t)) \sum_{\beta} \frac{\partial \mu_{\beta}}{\partial t} \\ & \quad \times \Delta \left(\Delta V_{\alpha} \Delta V_{\beta} \right) \left(\sum_{\gamma=1}^{\text{cliques}} \mu_{\gamma}(t) V_{\gamma}(x) \right) dx \\ & - \int \tilde{p}(x; \mu(t)) \sum_{\beta} \frac{\partial \mu_{\beta}}{\partial t} \\ & \quad \times \Delta \left(\Delta V_{\alpha} \Delta V_{\beta} \right) \log Z(\mu(t)) dx \\ & - \int \tilde{p}(x; \mu(t)) \sum_{\beta} \frac{\partial \mu_{\beta}}{\partial t} \\ & \quad \times \Delta \left(\Delta V_{\alpha} \Delta V_{\beta} \right) \log p(x; t) dx. \end{aligned}$$

In the second of these terms, the factor $\log Z(\mu(t))$ is not a function of x . As a result, when the integral is evaluated, the resulting expected values all cancel. So this term is zero, leaving

$$\begin{aligned} & \int (B + C + D) \frac{\partial}{\partial t} A dx \\ &= - \int \tilde{p}(x; \mu(t)) \sum_{\beta} \frac{\partial \mu_{\beta}}{\partial t} \\ & \quad \times \Delta \left(\Delta V_{\alpha} \Delta V_{\beta} \right) \left(\sum_{\gamma=1}^{\text{cliques}} \mu_{\gamma}(t) V_{\gamma}(x) \right) dx \\ & - \int \tilde{p}(x; \mu(t)) \sum_{\beta} \frac{\partial \mu_{\beta}}{\partial t} \\ & \quad \times \Delta \left(\Delta V_{\alpha} \Delta V_{\beta} \right) \log p(x; t) dx. \end{aligned} \quad (26)$$

Once again, we break apart equation (26) and consider the parts individually. Beginning with the first integral, we regroup the terms of the multiplication so

that there is just one double-sum over cliques, then move terms which do not depend on x outside of the integral, and integrate. This leaves another expected value:

$$\begin{aligned} & - \int \tilde{p}(x; \mu(t)) \sum_{\beta} \frac{\partial \mu_{\beta}}{\partial t} \Delta \left(\Delta V_{\alpha} \Delta V_{\beta} \right) \\ & \quad \times \left(\sum_{\gamma=1}^{\text{cliques}} \mu_{\gamma}(t) V_{\gamma}(x) \right) dx \\ &= - \sum_{\beta=1}^{\text{cliques}} \sum_{\gamma=1}^{\text{cliques}} \mu_{\gamma}(t) \\ & \quad \times \frac{\partial \mu_{\beta}(t)}{\partial t} \left\langle V_{\gamma} \Delta \left(\Delta V_{\alpha} \Delta V_{\beta} \right) \right\rangle. \end{aligned} \quad (27)$$

This expression belies some of the symmetry of this term. Note that, if $X = V_{\gamma}$ and $Y = \left(\Delta V_{\alpha} \Delta V_{\beta} \right)$, the inner most term is $\langle X \Delta Y \rangle$. From the definitions of Δ and expectation, this is equivalent to $\langle XY \rangle - \langle X \rangle \langle Y \rangle$, which once again is $\text{Cov}(X, Y)$. Of course, covariance relationships are symmetric, so this is also $\text{Cov}(Y, X)$, which from the preceding argument is $\langle Y \Delta X \rangle$. Thus

$$\langle X \Delta Y \rangle = \text{Cov}(X, Y) = \langle Y \Delta X \rangle. \quad (28)$$

Applying this transformation to equation (27), we have finally

$$\begin{aligned} & - \sum_{\beta=1}^{\text{cliques}} \sum_{\gamma=1}^{\text{cliques}} \mu_{\gamma}(t) \frac{\partial \mu_{\beta}(t)}{\partial t} \left\langle V_{\gamma} \Delta \left(\Delta V_{\alpha} \Delta V_{\beta} \right) \right\rangle \\ &= - \sum_{\beta=1}^{\text{cliques}} \sum_{\gamma=1}^{\text{cliques}} \mu_{\gamma}(t) \frac{\partial \mu_{\beta}(t)}{\partial t} \left\langle \Delta V_{\alpha} \Delta V_{\beta} \Delta V_{\gamma} \right\rangle. \end{aligned} \quad (29)$$

Turning to the second half of equation (26), the steps are similar, but the V_{γ} terms are replaced with $\log p(x)$ terms:

$$\begin{aligned} & - \int \tilde{p}(x; \mu(t)) \sum_{\beta} \frac{\partial \mu_{\beta}}{\partial t} \\ & \quad \times \Delta \left(\Delta V_{\alpha} \Delta V_{\beta} \right) \log p(x; t) dx \\ &= - \sum_{\beta=1}^{\text{cliques}} \frac{\partial \mu_{\beta}(t)}{\partial t} \left\langle \Delta V_{\alpha} \Delta V_{\beta} \Delta \log p(x; t) \right\rangle. \end{aligned} \quad (30)$$

The final piece of equation (23) is

$$\begin{aligned} \int A \frac{\partial}{\partial t} D dx &= \int \tilde{p}(x; \mu(t)) \left(V_{\alpha}(x) \right. \\ & \quad \left. - \langle V_{\alpha} \rangle \right) \frac{\partial}{\partial t} \log p(x; t) dx \\ &= \left\langle \Delta V_{\alpha} \frac{\partial}{\partial t} \log p(x; t) \right\rangle. \end{aligned} \quad (31)$$

Now that we have analyzed each of the parts of equation (23), we can set it equal to zero and move the terms with a sum over cliques across the equals sign. Then we have as a solution

$$\begin{aligned}
& \left\langle \Delta V_\alpha \frac{\partial}{\partial t} \log(p(x; t)) \right\rangle \\
&= \sum_{\beta=1}^{\text{cliques}} \frac{\partial \mu_\beta(t)}{\partial t} \\
&\quad \times \left(\left\langle \Delta V_\alpha \Delta V_\beta \Delta \log(p(x; t)) \right\rangle \right. \\
&\quad - \left\langle \Delta V_\alpha \Delta V_\beta \right\rangle \\
&\quad \left. + \sum_{\gamma=1}^{\text{cliques}} \mu_\gamma(t) \left\langle \Delta V_\alpha \Delta V_\beta \Delta V_\gamma \right\rangle \right). \quad (32)
\end{aligned}$$

Following the master equation for the derivative of p , and setting $\partial \mu_\beta(t)/\partial t \equiv f_\beta(\mu(t))$ this expression becomes

$$\begin{aligned}
& \left\langle \Delta V_\alpha \frac{(W \cdot p(; t))(x)}{p(x; t)} \right\rangle = \sum_{\beta=1}^{\text{cliques}} f_\beta(\mu(t)) \\
&\quad \times \left(\left\langle \Delta V_\alpha \Delta V_\beta \Delta \log p(x; t) \right\rangle - \left\langle \Delta V_\alpha \Delta V_\beta \right\rangle \right. \\
&\quad \left. + \sum_{\gamma=1}^{\text{cliques}} \mu_\gamma(t) \left\langle \Delta V_\alpha \Delta V_\beta \Delta V_\gamma \right\rangle \right).
\end{aligned}$$

Then, using equation (12) to define a linear form for f_β , we have

$$\begin{aligned}
& \left\langle \Delta V_\alpha \frac{(W \cdot p(; t))(x)}{p(x; t)} \right\rangle = \sum_{\beta=1}^{\text{cliques bases}} \sum_{A=1} \theta_{\beta A} f_A(\mu(t)) \\
&\quad \times \left(\left\langle \Delta V_\alpha \Delta V_\beta \Delta \log p(x; t) \right\rangle - \left\langle \Delta V_\alpha \Delta V_\beta \right\rangle \right. \\
&\quad \left. + \sum_{\gamma=1}^{\text{cliques}} \mu_\gamma(t) \left\langle \Delta V_\alpha \Delta V_\beta \Delta V_\gamma \right\rangle \right).
\end{aligned}$$

The p expressions in numerator and denominator may be evaluated using the BMLA-trained approximation of $p(x, t)$ at time t . Then, these expressions are finally in a form which can be evaluated during Monte Carlo simulations of \tilde{p} , resulting in an online learning algorithm in the spirit of BMLA itself, though more complicated. To this end we now define a vector \mathbf{B} with α entries

$$\mathbf{B}_\alpha = \left\langle \Delta V_\alpha \frac{(W \cdot p(; t))(x)}{p(x; t)} \right\rangle, \quad (33)$$

and a structured α -by- (β, A) matrix \mathbf{A} with entries

$$\begin{aligned}
\mathbf{A}_{\alpha, (\beta, A)} &= f_A(\mu(t)) \\
&\quad \times \left(\left\langle \Delta V_\alpha \Delta V_\beta \Delta \log p(x; t) \right\rangle \right.
\end{aligned}$$

Then $\mathbf{B} = \mathbf{A} \cdot \boldsymbol{\theta}$, where the dot product is taken over the compound index (β, A) . Finally, by calculating values for \mathbf{A} and \mathbf{B} we can solve for optimal $\boldsymbol{\theta}$.

It will generally be true that this system of equations is under-determined, as the dimensions of the matrix \mathbf{A} are $n \times (n \times m)$, where n is the number of potentials in the MRF and m is the total number of bases, and vector \mathbf{B} has length n . Therefore, it is useful to build larger \mathbf{A} and \mathbf{B} matrices by *stacking* together in a block fashion several copies of equations (33) and (34) together which have been computed using different distributions p and \tilde{p} , coming from different initial conditions or other input conditions as suggested in the operator approximations of equations (2) and (4), and characterized by different values of μ . As long as these copies are linearly independent this procedure can produce a fully constrained system of equations.

References

- [1] Pepke S, Kinzer-Ursem T, Mihalas S and Kennedy M B 2010 Dynamic model of interactions of Ca^{2+} , calmodulin, and catalytic subunits of Ca^{2+} /calmodulin-dependent protein kinase: II. *PLoS Comput. Biol.* **6** e1000675
- [2] Mjolsness E and Yosiphon G 2006 Stochastic process semantics for dynamical grammars *Ann. Math. Artif. Intell.* **47** 329–95
- [3] Kerr R A, Bartol T M, Kaminsky B, Dittrich M, Chang J C J, Baden S B, Sejnowski T J and Stiles J R 2008 Fast Monte Carlo simulation methods for biological reaction-diffusion systems in solution and on surfaces *SIAM J. Sci. Comput.* **30** 3126
- [4] Mjolsness E 2013 Time-ordered product expansions for computational stochastic systems biology *Phys. Biol.* **10** 035009
- [5] Hlavacek W S, Faeder J R, Blinov M L, Posner R G, Hucka M and Fontana W 2006 Rules for modeling signal-transduction systems *Science's STKE* **2006** re6
- [6] Danos V and Laneve C 2004 Formal molecular biology *Theor. Comput. Sci.* **325** 69–110
- [7] Gillespie D T 1977 Exact stochastic simulation of coupled chemical reactions *J. Phys. Chem.* **81** 2340–61
- [8] Kennedy M B, Beale H C, Carlisle H J and Washburn L R 2005 Integration of biochemical signalling in spine *Nat. Rev. Neurosci.* **6** 423–34
- [9] Yavneh I 2006 Why multigrid methods are so efficient *Comput. Sci. Eng.* **8** 12–22
- [10] Brandt A 1977 Multi-level adaptive solutions to boundary-value problems *Math. Comput.* **31** 333–90
- [11] Smyth P 1997 Belief networks, hidden Markov models, and Markov random fields: a unifying view *Pattern Recognit. Lett.* **18** 1261–8
- [12] Ackley D H, Hinton G E and Sejnowski T J 1985 A learning algorithm for Boltzmann machines *Cogn. Sci.* **9** 147–69
- [13] Johnson T 2012 Dependency diagrams and graph-constrained correlation dynamics: new systems for probabilistic graphical modeling *PhD Thesis* UC Irvine Computer Science Department. Available at URL <http://ics.uci.edu/~johnsong/thesis/>
- [14] Gillespie D T 1996 The multivariate Langevin and Fokker-Planck equations *Am. J. Phys.* **64** 1246–57
- [15] Lee C H, Kim K-H and Kim P 2009 A moment closure method for stochastic reaction networks *J. Chem. Phys.* **130** 1341–7

- [16] Schnoerr D, Sanguinetti G and Grima R 2014 Validity conditions for moment closure approximations in stochastic chemical kinetics *J. Chem. Phys.* **141** 084103
- [17] Gandhi A, Levin S and Orszag S 2000 Moment expansions in spatial ecological models and moment closure through Gaussian approximations *Bull. Math. Biol.* **62** 595–632
- [18] Risken H 1989 *The Fokker–Planck Equation* 2nd edn (Berlin: Springer)
- [19] Gillespie D T 2000 The chemical Langevin equation *J. Chem. Phys.* **113** 297
- [20] Sotiropoulos V, Contou-Carrere M-N, Daoutidis P and Kaznessis Y N 2009 Model reduction of multiscale chemical Langevin equations: a numerical case study *IEEE/ACM Trans. Comput. Biol. Bioinformatics* **6** 470–82
- [21] Singer A 2004 Maximum entropy formulation of the Kirkwood superposition approximation *J. Chem. Phys.* **121** 3657–66
- [22] Raghbi M, Hill N A and Dieckmann U 2011 A multiscale maximum entropy moment closure for locally regulated space–time point process models of population dynamics *J. Math. Biol.* **62** 605–53
- [23] Markham D C, Baker R E and Maini P K 2014 Modelling collective cell behavior *Discrete Continuous Dyn. Syst.* **34** 5123–33
- [24] Hespanha J 2008 Moment closure for biochemical networks *3rd Int. Symp. on Communications, Control and Signal Processing (ISCCSP)*
- [25] van Kampen N 1992 *Stochastic Processes in Physics and Chemistry* (Amsterdam: North Holland)
- [26] Singh A and Hespanha J P 2006 Lognormal moment closures for biochemical reactions *Proc. 45th IEEE Conf. on Decision and Control (San Diego, December 13–15)* pp 2063–8
- [27] Alexander F J, Johnson G, Eyink G L and Kevrekidis I G 2008 Equation-free implementation of statistical moment closures *Phys. Rev. E* **77** 26701
- [28] Rao C and Arkin A P 2003 Stochastic chemical kinetics and the quasi-steady-state assumption: application to the Gillespie algorithm *J. Chem. Phys.* **118** 4999–5010
- [29] Sinitsyn N A, Hengartner N and Nemenman I 2009 Adiabatic coarse-graining and simulations of stochastic biochemical networks *Proc. Natl Acad. Sci. USA* **106** 10546–51
- [30] Kang H W and Kurtz T G 2013 Separation of time-scales and model reduction for stochastic reaction networks *Ann. Appl. Probab.* **23** 529–83
- [31] Munsky B and Khammash M 2006 The finite state projection algorithm for the solution of the chemical master equation *J. Chem. Phys.* **124** 044104
- [32] Lebedz D, Skanda D and Fein M 2008 Automatic complexity analysis and model reduction of nonlinear biochemical systems *Computational Methods in Systems Biology (Lecture Notes in Computer Science vol 5307)* (Berlin: Springer) pp 123–40
- [33] Hangos K M, Gabor A and Szederkenyi G 2013 Model reduction in bio-chemical reaction networks with Michaelis–Menten kinetics *Proc. 2013 European Control Conf. (ECC) (Zurich, Switzerland)*
- [34] Rao S, van der Schaft A, van Eunen K, Bakker B M and Jayawardhana B 2014 A model reduction method for biochemical reaction networks *BMC Syst. Biol.* **8** 52
- [35] Feret J, Henzinger T, Koepl H and Petrov T 2012 Lumpability abstractions of rule-based systems *Theor. Comput. Sci.* **431** 137–64
- [36] Friedman J, Hastie T and Tibshirani R 2010 Regularization Paths for generalized linear models via coordinate descent *J. Stat. Softw.* **33** 1–22
- [37] Destexhe A, Mainen Z F and Sejnowski T J 1994 Synthesis of models for excitable membranes, synaptic transmission and neuromodulation using a common kinetic formalism *J. Comput. Neurosci.* **1** 195–230